ACI STRUCTURAL JOURNAL TECHNICAL PAPER

Title no. 110-S28

Experimental Study of Drop-Panel Effects on Response of Reinforced Concrete Flat Slabs after Loss of Corner Column

by Kai Qian and Bing Li

Flat-slab structures—with or without drop panels—are popular construction types and have a high occupancy rate. Such flat-slab structures are more vulnerable to progressive collapse compared to beam-column-slab structures, as there are no beams that could assist in redistributing the load previously carried by the lost column. Therefore, more efforts should be taken to assess the vulnerability of flat-slab structures to resist progressive collapse. Unfortunately, few experimental studies have been conducted on this subject to date. Thus, to attain a more comprehensive understanding of the behavior of reinforced concrete (RC) flat slabs in resisting progressive collapse and to quantify the influence of the drop panel on the performance of flat slabs against progressive collapse, two series (ND and WD) of one-third-scale specimens were tested under monotonic loading to simulate axial loading in the corner column. The experimental results highlighting the behavior, such as force-displacement responses, crack patterns, and failure mechanisms, are discussed. A comparison of the performance of these two series of specimens revealed that incorporating drop panels into the flat slabs would increase the first peak-resistant capacity by up to 124.7% and significantly reduce the likelihood of progressive collapse.

Keywords: corner; drop panel; flat slab; progressive collapse; reinforced concrete.

INTRODUCTION

Progressive collapse is defined by ASCE/SEI 7[1] as "the spread of an initial local failure from element to element, eventually resulting in the collapse of an entire structure or a disproportionately large part of it." Although progressive collapse is a low-probability phenomenon, the injuries and losses incurred in the event that it takes place could be very severe. Design guidelines[2,3] have proposed design procedures to evaluate the likelihood of progressive collapse of a structure following the notional removal of vertical load-bearing elements (columns and walls). Resistance to progressive collapse is achieved either implicitly—by provisions of minimum levels of strength, continuity, and ductility—or explicitly by: 1) providing alternate load paths so local damage is absorbed and major collapse is averted; or 2) providing sufficient strength to structural members that are critical to global stability. The alternate load path method is also frequently used to design structures in resisting progressive collapse due to its independence of abnormal loading conditions. According to this approach, if a primary load-bearing element, such as a column or wall, is destroyed during an extreme loading event, an alternate load path must be generated to redistribute the load initially carried by the lost columns or walls. To study the behavior of a reinforced concrete (RC) frame after the removal of one or more columns, several researchers[4,5] studied the performance of an RC frame following the loss of a column via numerical and analytical approaches, while Sasani and Sagiroglu,[6] Yi et al.,[7] Orton et al.,[8] Su et al.,[9] Yap and Li,[10] Tian and Su,[11] and Qian and Li[12-14] experimentally investigated the RC frame against progressive collapse. These studies have significantly improved the state-of-the-art standard of protective design and added to the database on progressive collapse behavior of RC structures.

However, the majority of the previous tests focused only on beam-column subassemblages without including the slabs or beam-column-slab substructures. In typical flat-slab or flat-plate structures, no beams contributed to the redistribution of the load previously borne by the lost corner column. Thus, they have greater vulnerability to progressive collapse compared to the beam-column-slab structures. Moreover, flat-slab and flat-plate structures are popular structure types and have a high occupancy rate. Hence, it is important to determine the extent of vulnerability of these structures in the event of column removal.[15] Unfortunately, few experimental studies have been conducted on this subject to date. Thus, to attain a more comprehensive understanding of the behavior of RC flat slabs in resisting progressive collapse and to quantify the influence of the drop panel on the performance of flat slabs against progressive collapse, two series of RC flat slabs—referred to as the "ND" (flat slab without drop panel) and "WD" (flat slab with drop panel) series—were tested at Nanyang Technological University (NTU), Singapore. By comparing the failure mechanisms and load-displacement responses of these two series of specimens, the effects of the drop panel on the performance of RC flat-slab structures can be determined.

RESEARCH SIGNIFICANCE

The performance of RC flat slabs—with or without drop panels—in resisting progressive collapse caused by the loss of a corner column was evaluated in this study. The primary objective of this paper is to study the drop-panel effects on the vertical load-displacement relationship, crack pattern, and failure mechanism of the flat slabs by comparing the test results. This study can help structural engineers gain a further understanding of the resistance mechanism of flat-slab structures against progressive collapse and provide evidence for the validation of existing numerical modeling approaches.

EXPERIMENTAL PROGRAM

Design of test setup

It is well-known that progressive collapse events are dynamic phenomena. In-place tests represent the preferred

ACI Structural Journal, V. 110, No. 2, March-April 2013.

Kai Qian *is a Research Associate at the Natural Hazards Research Centre (NHRC) at Nanyang Technological University, Singapore. He received his BEng (Hons) from Chang'an University, Xi'an, China, and his MSC and PhD from Nanyang Technological University. His research interests include the design of reinforced concrete structures, particularly in the area of progressive collapse.*

ACI member **Bing Li** *is an Associate Professor and Director at NHRC at Nanyang Technological University. He received his PhD from the University of Canterbury, Christchurch, New Zealand. His research interests include reinforced concrete and precast concrete structures, particularly in design for earthquake and blast resistance.*

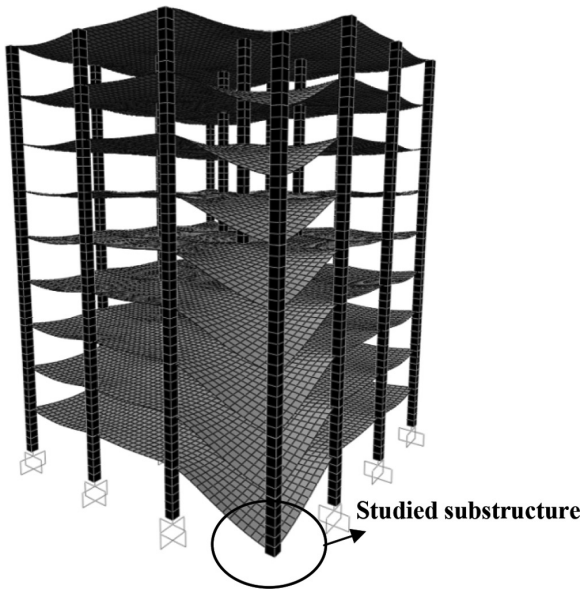

Fig. 1—Deformation shape of prototype flat plate after one of the corner columns was lost (drawing not to scale).

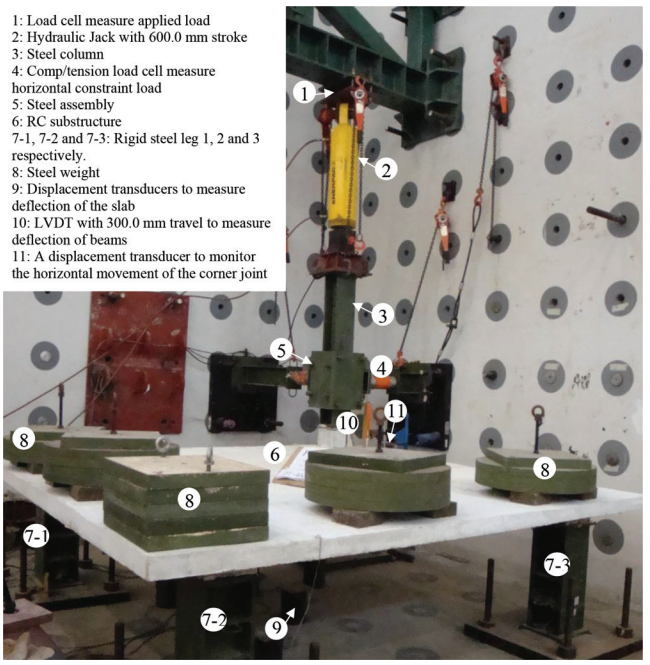

Fig. 2—Overview of typical specimen in position ready for testing. (Note: 1 mm = 0.0393 in.)

method to study the behavior of RC flat-slab structures for progressive collapse; however, the tremendous costs of the in-place tests mean that it is impossible to systematically investigate the behavior of RC flat-slab structures against progressive collapse via this method. The experimental results of Sasani and Sagiroglu[6] and Yi et al.[7] indicated that the upper and lower floors operate in tandem as a unit as long as the dimensions and reinforcement details in each floor are similar. Thus, the behavior of a multi-story frame could be simplified to that of a single-story substructure with proper boundary conditions. Figure 1 demonstrates the deformation shape of a nine-story flat-slab structure after one of the ground corner columns was lost. As shown in the figure, the deformation was concentrated in the corner panels. Therefore, one typical critical panel (the corner panel in the second story) was extracted and studied. A schematic of the test setup is shown in Fig. 2. Three rigid steel legs were used to support the slab and each steel leg was connected with a 75.0 mm (2.95 in.) thick strong plate through four ϕ27 bolts. The steel plates were fastened to the strong floor using pretensioned steel rods. Although major deformation was concentrated in the corner panel and limited deformation was observed in the adjacent bays following the removal of a corner column, the continuity of the slab could provide additional constraints on the slab and affect the realism of the test results. To partially simulate the influence of the continuity of the slabs on the overall performance, the slab was extended beyond the fixed support by one-fourth of the span in both directions. Five steel weight assemblies were applied on the extended part of the slab to simulate the influence of the continuity of surrounding slabs on the response of the specimens. It should be noted that the weight of the steel assemblies was determined by assuming that the design service pressure was applied on the extended parts. Before it was lost, the existing axial load in the corner column was simulated by applying downward displacements at the corner column stub through a hydraulic jack with a 600.0 mm (23.62 in.) stroke.

Sasani and Sagiroglu[6] identified three-dimensional (3-D) Vierendeel action as the major mechanism for the redistribution of loads in the framed structures under the scenario of the loss of a corner column; however, to date, there have not been any related in-place tests conducted for flat-slab structures. Thus, whether the Vierendeel action still dominates the load redistribution for a flat slab in the case of the loss of a corner column has not been fully understood. Thus, the numerical approaches[16] were used for this purpose. The numerical model was initially validated by the results obtained from Sasani et al.,[17] and the details of the numerical procedure can be found in Reference 18. The numerical results, as shown in Fig. 1, indicated that the column strips connected with the corner column deformed in double curvature after the removal of the corner column. Moreover, significant positive bending moment (tension at the bottom of the slab) was observed in the column strip local to the corner column after the removal of the corner column. Therefore, it can be concluded that the Vierendeel action still contributed to the load redistribution for flat slabs. Thus, to simulate the effect of the Vierendeel action applied on the test specimen,[12] the rotation of the corner column should be partially constrained. Figure 3 illustrates the details of the steel assembly used to apply the Vierendeel action equivalently to the tested specimens. One strong steel column was connected to the corner stub of the RC specimen using precast bolts. Four high-strength and high-stiffness steel pins were used to apply prescribed partial rotational and horizontal constraints in each direction. In other words, the steel column could move freely in the vertical direction, but its

rotational and horizontal freedoms were partially restrained. However, it should be pointed out that the extent of rotational constraint on the corner column for flat slabs should be different compared to that for beam-column-slab structures and the extent of this difference should be evaluated.

For test specimens, the numerical models[16] indicated that the center of the joint just above the lost column has a maximum outward horizontal movement of approximately 4.2 mm (0.17 in.), whereas the vertical displacement D_1 is approximately 180.0 mm (7.09 in.). It should be noted, however, that the rotational constraint assembly used in Qian and Li[12] was designed in accordance with the outward horizontal movement being 7.2 mm (0.28 in.) when the vertical displacement D_1 is approximately 180.0 mm (7.09 in.). Thus, the test results presented herein are slightly conservative, as the same rotational constraint assembly used in Qian and Li[12] was also used herein. The allowance between the steel pin and the hole was designed as follows

$$\phi = \frac{H_1}{TV} = \frac{H_1}{V + D_1} = \frac{7.2}{625 + 180} = 8.9 \times 10^{-3} \quad (1)$$

where ϕ is the design rotation of the steel column; H_1 is the horizontal movement of the center of the joint just above the damaged column; TV is the total vertical distance between the center of the steel box to the center of the corner joint when the specimen has a vertical displacement of D_1; V is the vertical distance between the center of the steel box to the center of the corner joint at the beginning of the test; and D_1 is the vertical displacement.

$$\delta = \frac{\overline{V} \times \phi}{2} = \frac{350 \times 8.9 \times 10^{-3}}{2} = 1.56 \quad (2)$$

where $\overline{V}$ is the average vertical distance between two steel pins in each direction; and δ is the difference between the diameter of the hole and the steel pin.

Therefore, the diameter of the steel pin was 40.0 mm (1.57 in.), while the diameter of the hole in the steel box was designed to be 43.0 mm (1.69 in.), as shown in Fig. 3.

Experimental substructures

Two series of column-slab substructures—referred to as the "ND" series (flat slab without drop panel) and "WD" series (flat slab with drop panels)—were constructed to study the effects of varying the amount of slab reinforcement in each series. The additional amount of resistance provided by incorporating the drop panels could be determined by comparison of the test results of these two series of specimens. The dimensions and reinforcement details are summarized in Table 1. As illustrated in the table, the only difference between WD1, WD2, and WD3 is the amount of the slab reinforcement. Figure 4 demonstrates the dimensions and reinforcement details in WD1. As shown in Fig. 4, the concrete cover of the column and slab are 20.0 and 7.0 mm (0.79 and 0.28 in.), respectively. For the WD series specimens, there is one corner column stub, three enlarged columns, and four drop panels cast monolithically. The corner column stub representing the removed column was a 200.0 mm (7.87 in.) square for all specimens, while the enlarged columns were 250.0 mm (9.84 in.) squares to ensure that failure would not occur in these enlarged columns. Moreover, the reinforcements were installed in both the top and bottom of the slab to prevent possible brittle failure of the specimen within

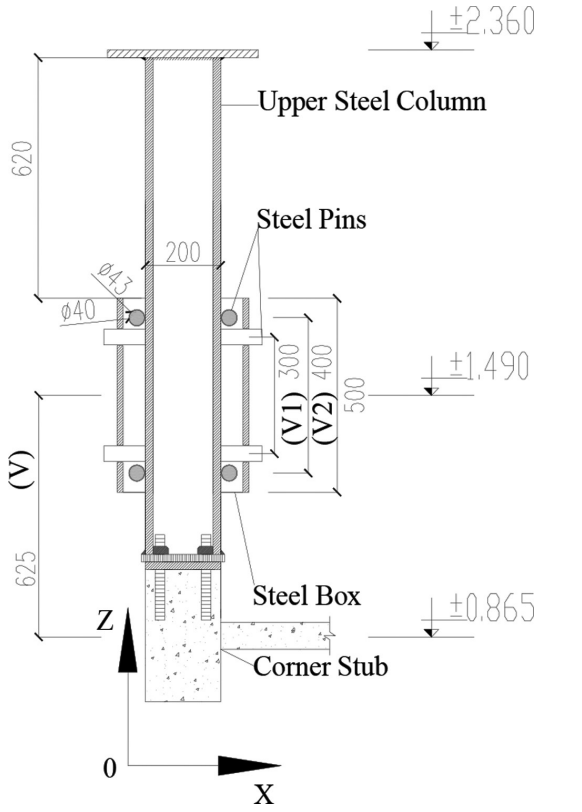

Fig. 3—Detailing of steel assembly (in mm). (Note: 1 mm = 0.0393 in.)

Table 1—Specimen properties

Test	Column stub	Slab thickness, mm	Slab top layer reinforcing bar		Slab bottom layer reinforcing bar		Drop-panel thickness	Drop panel reinforcing bar, mm	Design axial force, kN (kips)
			Column strip, mm	Middle strip, mm	Column strip, mm	Middle strip, mm			
ND1	Height = 400.0 mm Cross section = 200 x 200 Reinforcement ratio = 2.0%	70.0	R6 at 125	R6 at 250	R6 at 250	R6 at 250	None	None	15.9 (3.58)
ND2		70.0	R6 at 60	R6 at 125	R6 at 125	R6 at 125	None	None	15.9 (3.58)
ND3		70.0	R6 at 35	R6 at 70	R6 at 70	R6 at 70	None	None	15.9 (3.58)
WD1		70.0	R6 at 125	R6 at 250	R6 at 250	R6 at 250	40.0 mm	R6 at 70	15.9 (3.58)
WD2		70.0	R6 at 60	R6 at 125	R6 at 125	R6 at 125	40.0 mm	R6 at 70	15.9 (3.58)
WD3		70.0	R6 at 35	R6 at 70	R6 at 70	R6 at 70	40.0 mm	R6 at 70	15.9 (3.58)

Notes: 1 mm = 0.0393 in.; R6 is plain reinforcing bar with diameter of 6 mm.

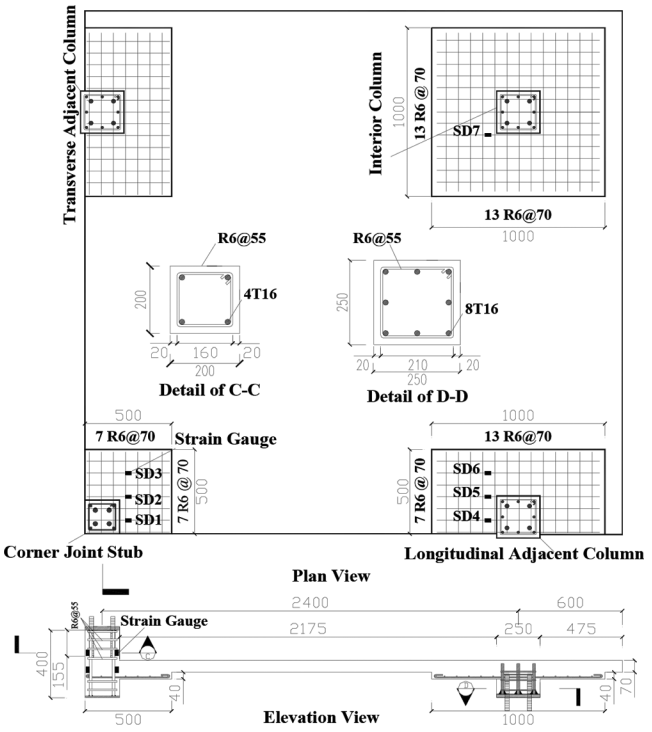

Fig. 4—Dimensions, cross-section details, and strain gauge locations of typical WD series specimens (in mm). (Note: 1 mm = 0.0393 in.; T is deformed reinforcing bar; R is plain reinforcing bar.)

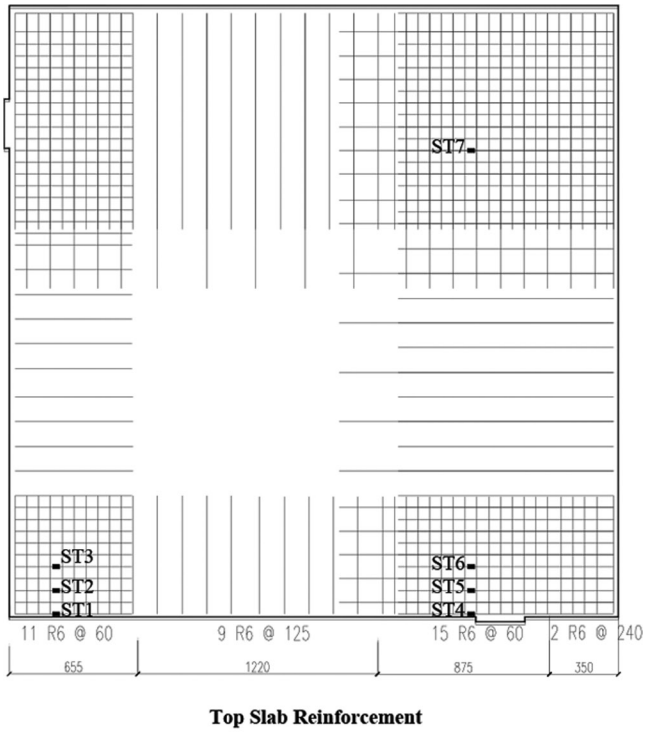

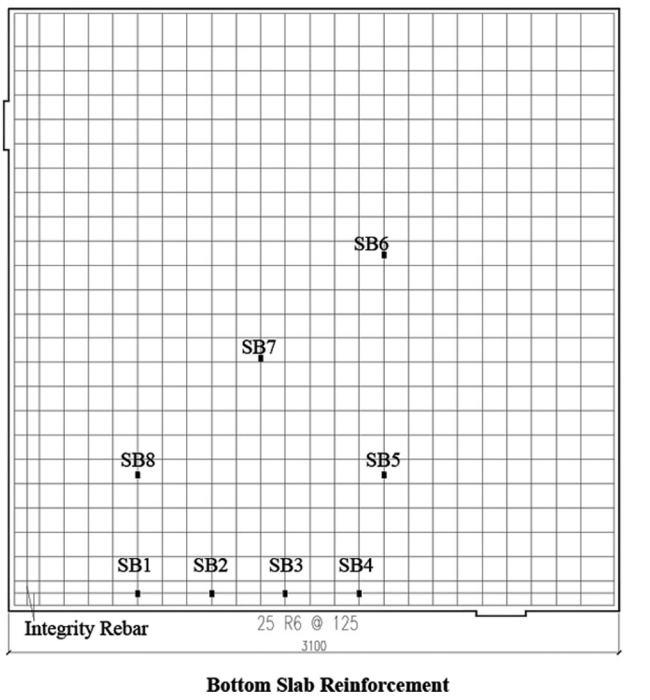

Fig. 5—Slab reinforcement details and strain gauge locations of Specimens ND2 and WD2 (in mm). (Note: 1 mm = 0.0393 in.)

the small deformation stage due to punching shear failure occurring in the column-slab connections. The thickness of the drop panel was 40.0 mm (1.57 in.) and the reinforcement in the drop panel was one layer reinforcing bar spaced at 70.0 mm (2.76 in.). Four ϕ25 bolts were precast in each enlarged column and connected with the steel legs. Figure 5 illustrates the slab reinforcement details of ND2 and WD2. As presented in Fig. 5, the slab reinforcement in the middle strip comprised the R6 reinforcing bar at 125.0 mm (4.92 in.) in two layers at the top and bottom, whereas the column strip was composed of two layers of R6 reinforcing bar spaced at 60.0 and 125.0 mm (2.36 and 4.92 in.) at the top and bottom, respectively.

Specimens ND1, ND2, and ND3 corresponded to WD1, WD2 and WD3, respectively. As shown in Table 1, similar details were provided in the columns and slabs of the ND series specimens as the corresponding WD series specimens, while no drop panels were incorporated. High-yield-strength steels were used for the longitudinal reinforcement (T16), while mild steel was used for the transverse and slab reinforcements (R6). It should be noted that T16 and R6 represent a deformed reinforcing bar with a diameter of 16 mm (0.63 in.) and a plain reinforcing bar with a diameter of 6 mm (0.24 in.), respectively. The average concrete compressive strengths were approximately 19.5 and 26.0 MPa (4.07×10^5 and 5.43×10^5 lb/ft^2) for the ND and WD series specimens, respectively. It should be noted that Prototype WD2 was designed in accordance with ACI 318-08.[19] The dead load (DL) of the prototype structure due to the 210.0 mm (8.26 in.) thick slab was 5.1 kPa (106.6 lb/ft^2). The additional DL was assumed to be 1.0 kPa (20.9 lb/ft^2). The equivalent additional DL due to the weight of infill walls was 2.25 kPa (47.0 lb/ft^2). The live load (LL) was assumed to be 2.0 kPa (41.8 lb/ft^2). One-third-scale substructures were cast and tested in this study. A uniform pressure of 11.0 kPa (229.7 lb/ft^2) based on the loading combination (1.2DL + 0.5LL), which is suggested in the Department of Defense[2] guidelines, was applied on the surface of the prototype slabs. To create the same demand/capacity ratio on the critical slab section of the scaled-down slabs as that of the prototype slabs, the same magnitude of pressure (11.0 kPa [229.9 lb/ft^2]) should be applied on the scaled-down slabs. The design axial force in the corner

Table 2—Test results

Test	First diagonal slab crack, kN (kips)	First yield load, kN (kips)	First peak capacity P_{cu}, kN (kips)	First punching failure, mm (in.)	Start to develop tensile membrane, mm (in.)	MCHR transverse direction, kN (kips)	MCHR longitudinal direction, kN (kips)	MTHR in transverse direction, kN (kips)	MTHR in longitudinal direction, kN (kips)	Second peak capacity, kN (kips)	Dynamic strength, kN (kips)	DLIF
ND1	6.3 (1.42)	7.3 (1.64)	8.5 (1.91)	410.9 (16.18)	120.3 (4.74)	4.5 (1.01)	4.5 (1.01)	6.0 (1.35)	6.1 (1.37)	17.3 (3.89)	6.9 (1.55)	1.23
ND2	9.1 (2.05)	11.6 (2.61)	14.3 (3.22)	380.9 (15.00)	131.3 (5.17)	4.2 (0.95)	5.7 (1.28)	7.3 (1.64)	8.1 (1.82)	18.5 (4.16)	11.8 (2.66)	1.21
ND3	13.4 (3.02)	20.0 (4.50)	22.4 (5.04)	50.4 (1.98)	120.8 (4.76)	6.6 (1.49)	5.2 (1.17)	11.0 (2.48)	9.5 (2.14)	24.8 (5.58)	18.6 (4.19)	1.20
WD1	10.2 (2.30)	15.4 (3.47)	19.1 (4.30)	None	221.3 (8.71)	8.5 (1.91)	9.0 (2.03)	9.0 (2.03)	7.9 (1.78)	24.6 (5.54)	16.0 (3.60)	1.19
WD2	14.3 (3.22)	22.0 (4.95)	26.8 (6.03)	None	200.0 (7.87)	9.5 (2.14)	10.4 (2.34)	9.5 (2.14)	9.0 (2.03)	32.5 (7.31)	23.1 (5.20)	1.16
WD3	17.1 (3.85)	32.2 (7.25)	36.2 (8.15)	None	221.3 (8.71)	10.9 (2.45)	11.9 (2.68)	13.9 (3.13)	12.5 (2.81)	40.3 (9.07)	32.1 (7.22)	1.13

Notes: MCHR and MTHR are maximum compressive horizontal reaction force and maximum tensile horizontal reaction force, respectively; DLIF is dynamic load increase factor, as ratio of static ultimate capacity to peak value measured in capacity curve.

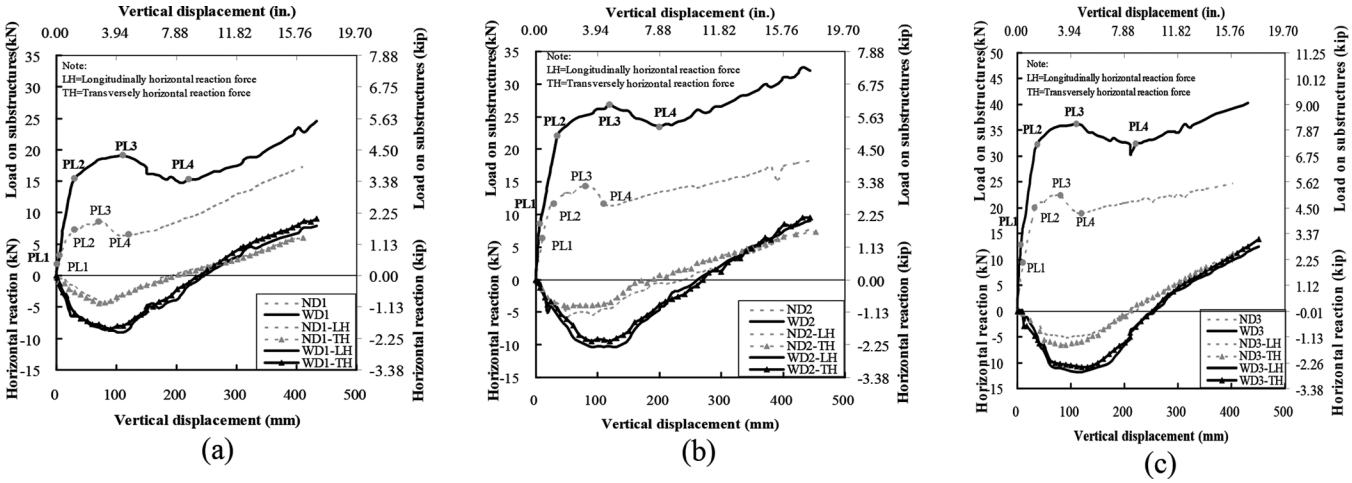

Fig. 6—Comparison of vertical load and horizontal reaction force versus vertical deflection (ND series specimens and corresponding WD series specimens).

column of each specimen, as recommended by the Department of Defense[2] guidelines, is listed in Table 1.

Instrumentation

Extensive measurement devices were installed both internally and externally to monitor the response of the test specimens. A total of 35 and 42 data channels were active during the testing process for the ND and WD series specimens, respectively. A load cell was used to measure the applied force on the corner stub. Two tensile and compressive load cells were horizontally connected with the steel assembly and used to measure the horizontal reaction of the box in each direction. One linear variable differential transformer (LVDT) with 300.0 mm (11.81 in.) travel was installed vertically to measure the vertical movement of the corner column stub during the test. To monitor the horizontal movement of the corner joint during the test, a displacement transducer with 1200.0 mm (47.24 in.) travel was installed horizontally. The remaining six displacement transducers were placed vertically to monitor the deflection of the slab. For the ND series specimens, a total of 23 strain gauges were mounted on the reinforcement at strategic locations to monitor the strain variation along the corner column and slab during the test. For the WD series specimens, strain gauges were not only installed in the column and slab but were also placed in the drop panels. The locations of the strain gauges placed in the drop panel and corner column are shown in Fig. 4, while the locations of the strain gauges in the slab reinforcement are illustrated in Fig. 5.

EXPERIMENTAL RESULTS OF COLUMN-SLAB SUBSTRUCTURES

Two series (ND and WD) of one-third-scale flat-slab substructures were constructed and tested to evaluate the drop-panel effects on the performance of flat slabs for progressive collapse caused by the loss of a ground corner column with different amounts of slab reinforcement. The key points of the test results of the six specimens are summarized in Table 2 and discussed in the following.

Global behavior

Specimen ND1—The measured vertical and horizontal reaction force versus the vertical displacement of the corner joint of Specimen ND1 with different performance levels is shown in Fig. 6(a). Four performance levels at significant parts of the test were identified. Performance Levels PL1, PL2, PL3, and PL4 represent the first flexural crack, the first

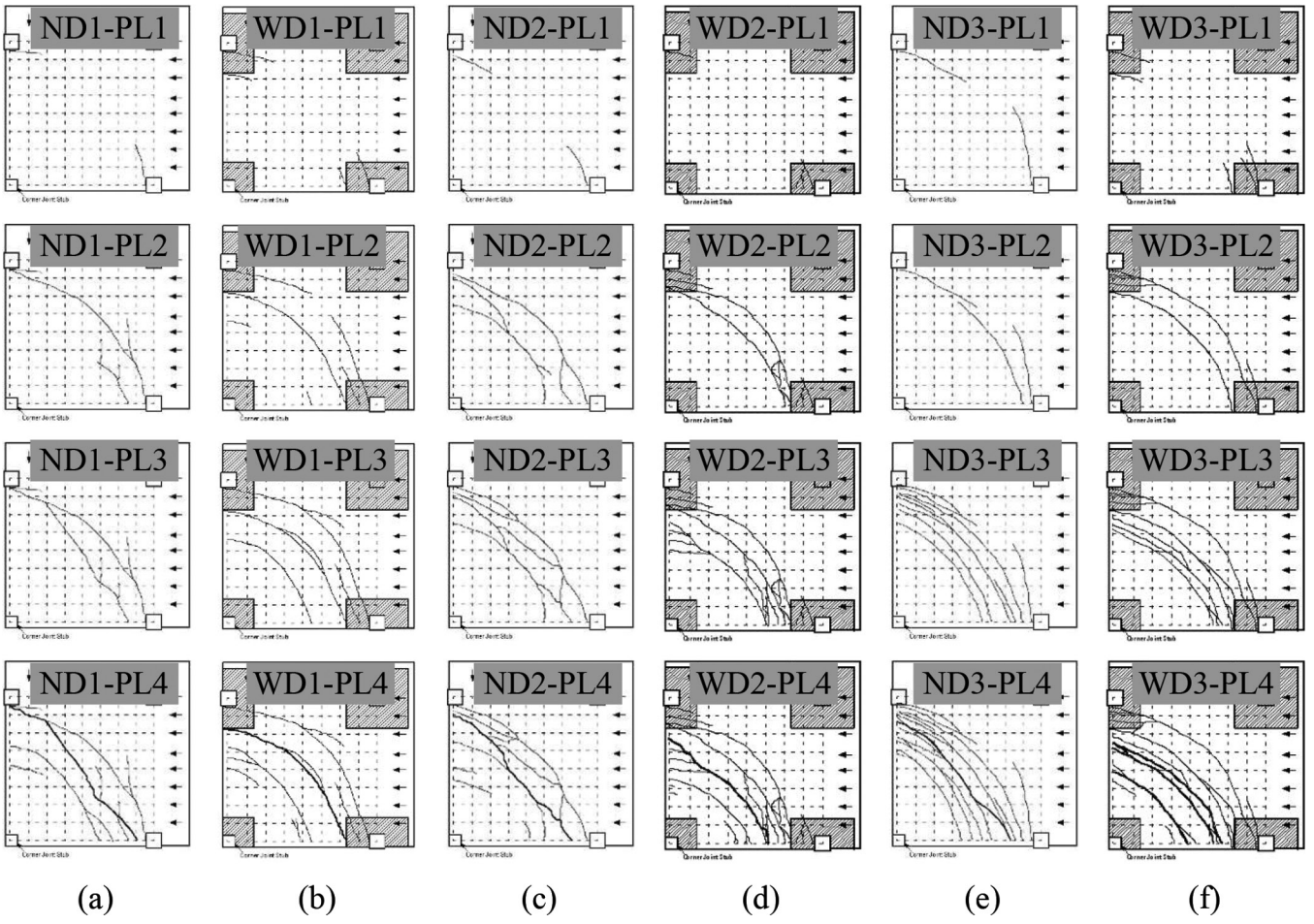

Fig. 7—Observed cracking patterns at different performance levels of test specimens.

yield of the slab reinforcement local to the enlarged adjacent column, the first peak capacity, and the beginning of the development of tensile membrane action, respectively. The first crack was observed at the interface between the slab and the adjacent enlarged column at a load of 1.8 kN (0.41 kips). Following the first crack, several flexural cracks were observed at the bottom of the slab close to the corner column due to equivalent Vierendeel action. At a load of 6.3 kN (1.42 kips), the first diagonal crack in the slab was formed and passed through the center of the slab. However, the first yield of the top reinforcement was observed at a load of 7.3 kN (1.62 kips) and corresponded to a vertical displacement of 30.9 mm (1.22 in.). When the vertical displacement reached 70.3 mm (2.77 in.), the first peak capacity P_{cu} was attained at a load of 8.5 kN (1.91 kips) and corresponded to 53.4% of the design axial load, as recommended by the Department of Defense.[2] At this load stage, more diagonal cracks parallel to the first diagonal crack were formed and these diagonal cracks moved toward the corner column. With further increase of the vertical displacement, the resistance of the specimen began to decrease due to severe yield of the slab reinforcement. When the displacement reached 120.3 mm (4.74 in.), which was equivalent to 4.2% of the tip displacement ratio (TDR)—defined as the ratio of vertical displacement at the center of the corner stub to column spacing—the load-displacement curve began to ascend again (attributable to tensile membrane action). A diagonal crack penetrated through the depth of the slab with a further increase in vertical displacement. At the end of the test, punching shear cracks were observed in the corner column-slab connection. It should be noted that no obvious punching failure was observed in the top slab around the adjacent columns. Figure 7(a) illustrates the crack pattern development corresponding to different performance levels of ND1. It should be pointed out that no cracks were observed in the corner column and joint region during the test. This was significantly different from the failure mode of the beam-column-slab substructures tested by Qian and Li.[12]

Both the transverse and longitudinal horizontal reaction forces were measured by the tension/compression load cells (Item 4 in Fig. 2), which were connected with the steel assembly. As shown in Fig. 6(a), the recorded horizontal compressive force was limited before the first crack occurred in the specimen; however, it significantly increased after the first crack was observed (similar behavior was observed by Qian and Li[12]). The recorded response of the horizontal reaction force in the transverse direction was almost identical to that measured in the longitudinal direction. A maximum compressive force of 4.1 and 4.5 kN (0.92 and 1.01 kips) was measured in the transverse and longitudinal directions at the displacements of 70.3 and 80.1 mm (2.77 and 3.15 in.), respectively. It should be noted that the measured compressive force did not represent the horizontal axial force developed in the center of the corner joint, as the majority of the compressive force was used to balance the positive bending moment at the slab-corner column connection. When the displacement reached 202.4 mm (7.97 in.), which was equivalent to 8.4% of the TDR, tensile reaction forces were

recorded in both horizontal load cells. At the final stage of the test, the maximum horizontal tensile reaction forces measured in the transverse and longitudinal load cells were 6.0 and 6.1 kN (1.35 and 1.37 kips), respectively.

Specimen WD1—The measured vertical and horizontal reaction force versus the vertical displacement of the corner joint of Specimen WD1 is shown in Fig. 6(a). At a load of 3.2 kN (0.72 kips), flexural cracks were initiated in the slab-adjacent column interfaces. A few flexural cracks were observed in the bottom of the drop panel around the corner column at a load of 7.6 kN (1.71 kips) due to equivalent Vierendeel action. At a load of 10.2 kN (2.30 kips), the first diagonal crack in the slab was formed. It should be pointed out that this diagonal crack was connected with the edges of the drop panels around the longitudinal and transverse adjacent columns, as the drop panels increased the moment capacity of the slab section near the adjacent column and shifted the most critical section from the slab-adjacent column interface to the edge of the drop panel. The first yield of the top reinforcement was observed at a load of 15.4 kN (3.47 kips) and corresponded to a vertical displacement of 30.0 mm (1.18 in.). When the vertical displacement reached 110.7 mm (4.36 in.), the first peak capacity P_{cu} was attained at a load of 19.1 kN (4.30 kips) and corresponded to 120.1% of the design axial load, as recommended by the Department of Defense.[2] The major diagonal crack in the slab became wider with a further increase in the vertical displacement. When the vertical displacement reached 130.0 mm (5.12 in.), concrete crushing was observed in the top slab local to the corner column. When the displacement reached 221.3 mm (8.71 in.), which was equivalent to 9.2% of the TDR, the load-displacement curve began to ascend again (attributable to tensile membrane action). Compared with Specimen ND1, no obvious punching failure was observed in the corner column-slab connection during the test due to the drop panel significantly increasing the effective depth of the slab. Similar to ND1, however, severe flexural cracks were formed in the bottom surface of the corner drop panel when the vertical displacement reached 350.0 mm (13.8 in.). In addition, similar to ND1, no cracks were observed in the corner column and joint during the test. Figure 7(b) illustrates the crack pattern development at different performance levels for WD1. The maximum compressive forces of 8.5 and 9.0 kN (1.91 and 2.03 kips) were measured in the transverse and longitudinal directions at the displacements of 90.8 and 100.7 mm (3.57 and 3.96 in.), respectively. The maximum horizontal tensile reaction forces of 9.0 and 7.9 kN (2.03 and 1.78 kips) were measured in the transverse and longitudinal directions at the final stage of the test, respectively.

Specimen ND2—The measured vertical and horizontal reaction force versus the vertical displacement of the corner joint of Specimen ND2 is shown in Fig. 6(b). In general, the crack development of ND2 was similar to that of ND1 and the key points of the test results are listed in Table 2. Thus, only the foremost discrepancies between these two specimens are emphasized herein. For ND1, the first diagonal crack in the slab was formed at a load of 6.3 kN (1.42 kips). For ND2, however, the diagonal crack in the slab was formed and passed through the center of the slab at a load of 9.1 kN (2.05 kips). Another difference between the crack patterns of ND2 and ND1 was that the punching failure occurred at the corner column-slab connection of ND2 at a displacement of 380.9 mm (15.00 in.), while it occurred in ND1 at the final stage of the test (410.9 mm [16.18 in.]). In general, the crack pattern in ND2 was much finer than that in ND1. In ND1, only several discrete diagonal cracks were formed; however, numerous cracks were observed in between the diagonal cracks in ND2. A higher slab reinforcement ratio provided in the slab significantly increased the first yield and first peak capacity of the specimen. The failure mode of ND2 is depicted in Fig. 8, while the crack pattern development of ND2 is illustrated in Fig. 7(c).

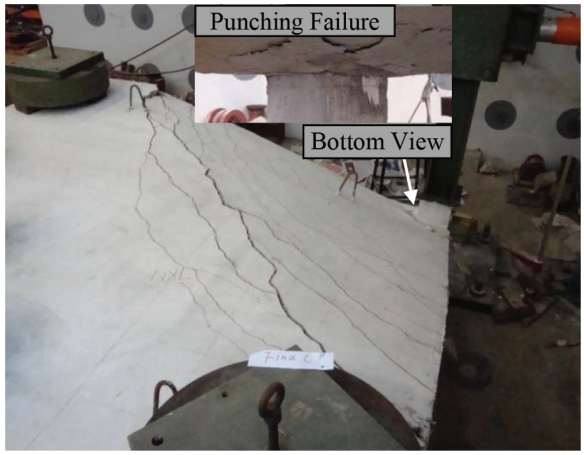

Fig. 8—Failure mode of Specimen ND2 at final.

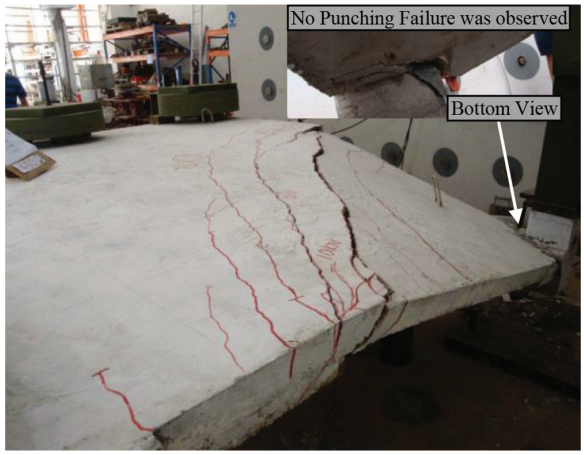

Fig. 9—Failure mode of Specimen WD2 at final.

Specimen WD2—The measured vertical and horizontal reaction force versus the vertical displacement of the corner joint of Specimen WD2 is shown in Fig. 6(b). In general, the crack development of WD2 was similar to that of WD1 and the key points of the test results are listed in Table 2. Thus, only the foremost discrepancies between these two specimens are emphasized. For WD1, the first diagonal crack in the slab was formed at a load of 10.2 kN (2.30 kips). For WD2, however, the diagonal crack was first formed and connected with the edges of the adjacent columns at a load of 14.3 kN (3.22 kips). Similar to ND2, the crack patterns observed in WD2 were much finer than those in WD1. Figure 9 depicts the failure mode of WD2, while Fig. 7(d) illustrates the crack pattern development corresponding to different performance levels of WD2.

Specimen ND3—The measured vertical and horizontal reaction force versus the vertical displacement of the corner joint of Specimen ND3 is shown in Fig. 6(c). In general, the crack development of ND3 was similar to that of ND1. For ND1, the first diagonal crack in the slab was formed at a load of 6.3 kN (1.42 kips). For ND3, however, the diagonal

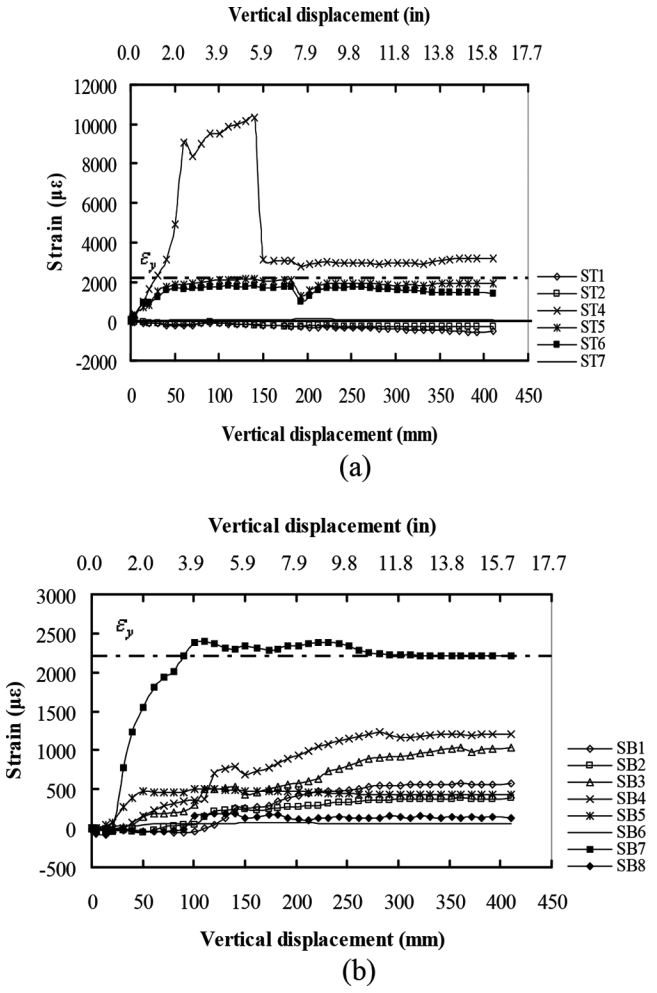

Fig. 10—Strain of slab reinforcement versus vertical displacement in Specimen ND1.

crack was formed and passed through the center of the slab at a load of 13.4 kN (3.02 kips). Another difference between the crack patterns of ND3 compared to those of ND1 was that the punching failure occurring in the corner column-slab connection of ND3 was first observed at a displacement of 50.4 mm (1.98 in.), which was before it reached its first peak capacity. However, although the sign of punching shear failure was observed before reaching the first peak capacity, this punching failure deteriorated slowly and did not prevent further redistribution of the load. This is possibly attributed to the special design—integrity reinforcements were installed in both the top and bottom of the slab (refer to Fig. 5). In general, the crack patterns in ND3 were much finer than those in either ND1 or ND2. The failure mode of ND3 was similar to ND2 and hence is not presented. The crack pattern development of ND3 is illustrated in Fig. 7(e).

Specimen WD3—The measured vertical and horizontal reaction force versus the vertical displacement of the corner joint of Specimen WD3 is shown in Fig. 6(c). The first diagonal crack in the slab was formed at loads of 10.2 and 14.3 kN (2.30 and 3.22 kips) for Specimens WD1 and WD2, respectively. For WD3, however, the diagonal crack in the slab was first formed at a load of 17.1 kN (3.85 kips). It should be pointed out that slight cracks were also observed in the corner joint and corner column at the final stage of the test for this specimen. The failure mode of WD3 was similar to that of WD2 and thus is not presented. Figure 7(f) illustrates the crack pattern development corresponding to different performance levels of WD3.

DISCUSSION OF TEST RESULTS AND DROP-PANEL EFFECTS

Comparison of performance of ND series specimens to corresponding WD series specimens

Load-displacement relationship—Figure 6 shows the comparison of the load-displacement relationship of the WD series specimens with the corresponding ND series specimens. By comparing the first peak capacity of the two specimens, it can be seen that Specimen ND1 can only reach 53.4% of the design axial load, as recommended by the Department of Defense,[2] while WD1 can reach 120.1% of the design axial load. The first peak capacity of WD1 was increased by approximately 124.7% compared with that of ND1. Based on the test results, 89.9% and 168.6% of the design axial load, as recommended by the Department of Defense,[2] could be achieved by ND2 and WD2, respectively. The first peak capacity of WD2 was enhanced by approximately 87.5% compared with ND2; however, Specimens ND2 and WD2 could attain the second peak-carrying capacities of 18.5 and 32.5 kN (4.16 and 7.31 kips), respectively, at the final stage of the test. For Specimens ND3 and WD3, 140.9% and 227.7% of the design axial load, as recommended by the Department of Defense,[2] could be achieved based on the test results. The first peak capacity of WD3 was increased by approximately 61.6% compared with ND3. Moreover, Specimens ND3 and WD3 could attain the second peak-carrying capacities of 24.8 and 40.3 kN (5.58 and 9.07 kips), respectively, at the final stage of the tests.

In this study, the initial stiffness was defined as the secant stiffness at the first yield strength. The initial stiffness of Specimens ND1, ND2, and ND3 was 0.24, 0.39, and 0.61 kN/mm (1.35, 2.25, and 3.47 kip/in.), respectively. For Specimens WD1, WD2, and WD3, the initial stiffness was 0.51, 0.63, and 0.86 kN/mm (2.92, 3.60, and 4.94 kip/in.), respectively. Thus, the flat slab incorporated with drop panels could increase the initial stiffness by up to 117.4%.

Energy dissipation—The survival of the structures subjected to the scenario of the loss of a column is related to their ability to dissipate the input energy. In this study, the definition of energy dissipation is the area under the load-displacement curve of each specimen. The dissipated energies of Specimens ND1and WD1 at the final stage of the test were 4.1 and 7.6 kN.m (36.3 and 67.3 kip-in.), respectively. For Specimens ND2 and WD2, the dissipated energies were 6.3 and 11.3 kN.m (55.8 and 100.1 kip-in.), respectively. However, the dissipated energies were 8.4 and 14.7 kN.m (74.4 and 130.2 kip-in.) for ND3 and WD3, respectively. Thus, the incorporated drop panels could increase the energy dissipation capacities by 85.4%, 79.4%, and 75.0% for WD1, WD2, and WD3, respectively.

Local behavior-reinforcing bar strains—Figure 10 illustrates the relationship of strain in the slab reinforcement versus vertical displacement of Specimen ND1. The locations of strain gauges are illustrated in Fig. 5. As shown in Fig. 10(a), Strain Gauges ST1 and ST2 were in compression during the test. The maximum compressive strains of ST1 and ST2 were –561 με and –298 με, respectively. This confirmed that the direction of the bending moment of the column strip connected with the corner column changed after the removal of the corner column due to the equivalent

Vierendeel action. Moreover, it indicated that the extent of the Vierendeel action was not slacked during the test due to the corner column and joint being relatively intact during the test. For beam-column-slab substructures, however, the Vierendeel action was sluggish with increasing damage of the corner joint.[12] Strain Gauge ST4 recorded the tensile strain of 2331 με and yielded when the vertical displacement reached 30.9 mm (1.22 in.). For ST5 and ST6, the measured maximum tensile strains were 2143 με and 1799 με, respectively. They were close to the yield strain, although they had not yielded; however, the measured maximum tensile strain of ST7 was 120 με and this proved that the majority of the force initially resisted by the damaged corner column was transferred to the adjacent columns, while negligible force was transferred to the interior column (a similar conclusion was reached by Qian and Li[12]).

Figure 10(b) depicts the relationship of strain in the slab bottom reinforcement versus the vertical displacement. The strain in all bottom reinforcements except Strain Gauges SB5 and SB6 was in compression initially but was altered to be in tension with the increase in the vertical displacement. The tensile strains in SB1, SB2, SB3, and SB4 were significantly increased when the displacement attained 100.2 mm (3.94 in.). A re-ascending branch was observed in the load-displacement curve at this displacement stage. The measured maximum tensile strains in SB7 and SB8 were 2143 με and 191 με, respectively. This was due to the fact that the major diagonal crack was passing over the center of the slab for ND series specimens. It should be emphasized that the strain in the column longitudinal reinforcement of ND1 was also measured. The maximum tensile strain and compressive strain measured in the column longitudinal reinforcement were 363 με and –209 με, respectively. This was consistent with the crack pattern observation—no cracks were observed in the column and joint regions (in the elastic region) during the test for ND1. For WD1, in general, the trends of the strain curves were similar to those of ND1 and thus are not repeated herein.

Figure 11 presents the strain of the reinforcement in the drop panel of WD1 versus the vertical displacement. The locations of these strain gauges were shown in Fig. 4. The measured maximum tensile strains in SD1, SD2, and SD3 were 2965 με (beyond the yield strain), 1674 με, and 988 με, respectively, due to equivalent Vierendeel action. However, compressive strains were measured in SD4, SD5, and SD6 and the maximum compressive strains in SD4, SD5, and SD6 were –295 με, –254 με, and –261 με, respectively.

Discussion of punching shear strength of corner column-slab connection

As observed in the cracking patterns of the test specimens, unpredicted punching shear cracks were formed in the ND series specimens. As mentioned previously, to study the behavior of the specimens with large deformation well, the tested flat slabs were designed not to fail by brittle punching shear. Table 3 summarizes the comparison of the measured punching shear resistance from tested specimens with the values predicted by the punching shear formulations of ACI 318-08,[19] Eurocode 2,[20] CEB-FIP MC90,[21] and DIN 1045-1.[22] The design formulations of the aforementioned design code for predicting the punching shear capacities can be found in Reference 23. According to the provisions of ACI 318-08[19] and Eurocode 2,[20] the punching shear capacity of the corner-slab connection was calculated assuming the critical section had both rectangular and circular perimeters. As shown in the table, according to ACI 318-08,[19] the punching shear capacity of the corner slab-column connection is significantly overestimated, whether the assumed perimeter is rectangular or circular. However, the predictions of the Eurocodes, especially for CEB-FIP MC90[21] and DIN 1045-1,[22] are much closer to the measured values than those of ACI 318-08.[19] This is mainly due to the fact that the ACI 318-08[19] punching shear formulation accounts for neither the role of the reinforcement ratio nor the size of the member. Guandalini et al.[24] concluded that the nominal punching shear strength decreases with decreasing flexural reinforcement ratios. Moreover, in general, the

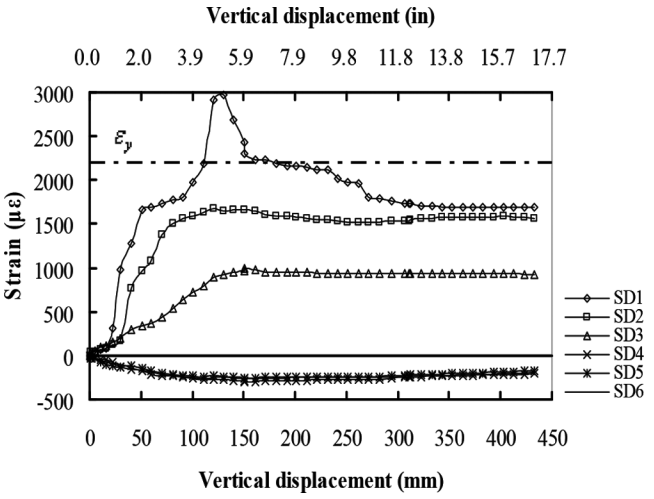

Fig. 11—Strain of reinforcing bar in drop panels of Specimen WD1 versus vertical displacement.

Table 3—Comparison of measured punching shear resistance with design codes

Test	V_{test}, kN (kips)	V^R_{ACI}, kN (kips)	V^S_{ACI}, kN (kips)	V^R_{EC2}, kN (kips)	V^S_{EC2}, kN (kips)	V^S_{CEB}, kN (kips)	V^S_{DIN}, kN (kips)	V_{Test}/V^R_{ACI}, kN (kips)	V_{Test}/V^S_{ACI}, kN (kips)	V_{Test}/V^R_{EC2}, kN (kips)	V_{Test}/V^S_{EC2}, kN (kips)	V_{Test}/V^S_{CEB}, kN (kips)	V_{Test}/V^S_{DIN}, kN (kips)
ND1	17.3 (3.89)	31.9 (7.18)	40.6 (9.14)	16.7 (3.77)	21.3 (4.80)	14.2 (3.20)	15.0 (3.42)	0.54	0.43	1.04	0.81	1.22	1.15
ND2	17.2 (3.87)	31.9 (7.18)	40.6 (9.14)	21.1 (4.75)	26.9 (6.05)	17.9 (4.04)	18.9 (4.30)	0.54	0.43	0.82	0.64	0.96	0.91
ND3	21.1 (4.72)	31.9 (7.18)	40.6 (9.14)	25.6 (5.76)	32.6 (7.32)	21.7 (4.89)	23.0 (5.23)	0.66	0.52	0.82	0.65	0.97	0.92
							Average	0.58	0.46	0.89	0.70	1.05	0.99

Notes: V^R_{ACI} and V^S_{ACI} are punching shear strength according to ACI 318-08[20] by considering control perimeters with rounded corners and straight corners, respectively; V^R_{EC2} and V^S_{EC2} are punching shear strength according to Eurocode 2[21] by considering control perimeters with rounded corners and straight corners, respectively; V^S_{CEB} and V^S_{DIN} are punching shear strength according to CEB-FIP MC90[22] and DIN 1045-1[23] by considering control perimeters with rounded corners and straight corners, respectively.

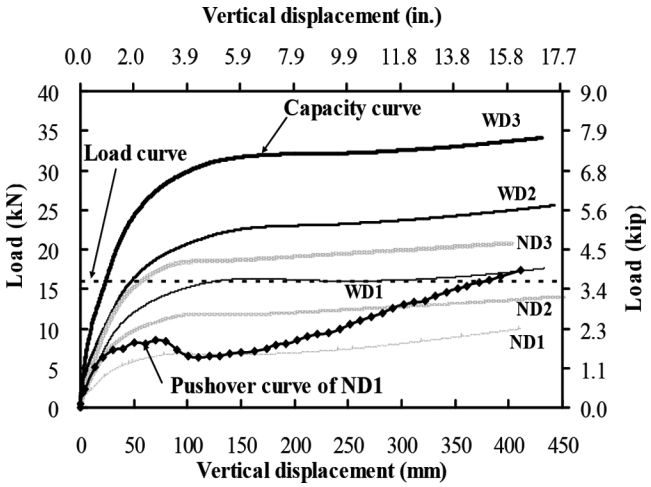

Fig. 12—Illustration of capacity curve and load curve of each specimen.

assumed circular perimeter gives a closer result to the calculations rather than the rectangular one.

Discussion of dynamic effect

As the design guidelines are still developing, the dynamic ultimate strength of each specimen was predicted by a simplified analytical model-capacity curve method in this paper. Then, the corresponding dynamic load increase factor (DLIF) of each specimen was determined. DLIF is defined herein as the ratio of static ultimate capacity to the dynamic ultimate capacity (the peak value of the capacity curve) of each specimen. The capacity curve method was proposed by Abruzzo et al.[25] based on the conservation of energy. After conducting nonlinear pushover analysis, the load-displacement curve of the structure can be obtained, where the area under this curve represents the strain energy in the structure. At the moment where the system achieves a balanced condition, this internal energy will be equal to the external work, defined as the product of the constant applied load (column axial force before damage) and the resulting displacement. If the system does not have adequate ductility to dissipate the required energy, the internal and external works will never balance each other and it will result in a collapse. Thus, a capacity curve may be constructed by dividing the accumulated stored energy by its corresponding displacement. However, it should be noted that the dissipated energy due to damping was not considered in this simplified mode. It is mathematically expressed as

$$P_{CC}(u_d) = \frac{1}{u_d}\int_0^{u_d} P_{NS}(u)du \tag{3}$$

where $P_{CC}(u_d)$ and $P_{NS}(u)$ are the capacity function and the nonlinear static loading estimated at the displacement demand u, respectively.

Figure 12 presents the capacity curve and load curve of each specimen. As seen from the figure, the load curves were the intersection of the capacity curves at the displacements of 137.8, 59.2, 50.8, and 24.8 mm (5.43, 2.33, 2.00, and 0.98 in.) for Specimens WD1, ND3, WD2, and WD3, respectively. Thus, these four specimens will not collapse, as energy balance can be achieved. However, the load curves in ND1 and ND2 were larger than the dynamic ultimate capacity of the corresponding specimens. Thus, both ND1 and ND2 will totally collapse if the corner support were removed suddenly. Taking ND1 as an example, significant tensile membrane action was observed in the load-displacement or pushover curve, as shown in Fig. 12. However, the increased dynamic ultimate capacity due to this tensile membrane action is very limited, as shown in Fig. 12. Thus, the contribution of the tensile membrane action in resisting the real dynamic progressive collapse event was probably not very reliable. The predicted ultimate capacity and corresponding DLIFs without considering the tensile membrane action are given in Table 2. As shown in the table, the predicted DLIF for the test specimens ranged from 1.13 to 1.23. The much lower dynamic effects on the ultimate capacity than that assumed in GSA[3] may be explained by the relatively ductile performance exhibited by the test specimens.

CONCLUSIONS

Based on the experimental study conducted in this research, the following conclusions were reached:

1. Experimental observation indicated that one of the potential failure modes for the flat-plate structures (ND series specimens) in resisting progressive collapse caused by the loss of a ground corner column was punching failure, which occurred in the corner column-slab connection. The deterioration of the punching failure was mild and the tests could be continued due to the installation of integrity reinforcement at both the top and bottom of the slab. In addition, the drop panels significantly mitigated the likelihood of such a kind of brittle failure mode. No punching shear cracks were observed in the WD series specimens.

2. As expected, the experimental results indicated that the incorporation of drop panels could significantly improve the overall performance in resisting progressive collapse. The first peak-carrying capacities of WD1, WD2, and WD3 (with a drop panel) were increased by 124.7%, 87.5%, and 61.6%, respectively, as compared to ND1, ND2, and ND3 (without a drop panel).

3. The experimental results indicated that a flat slab incorporated with a drop panel could increase the initial stiffness and energy dissipation capacity by up to 117.4% and 85.4%, respectively.

4. The amount of the slab reinforcement significantly affected the performance of the flat-slab structures in resisting progressive collapse. The first peak-carrying capacities increased by 68.2% and 163.5% in Specimens ND2 and ND3, respectively, compared to ND1. For Specimens WD2 and WD3, the first peak-carrying capacities increased by 40.3% and 89.5%, respectively, compared to WD1.

5. The re-ascending branch in the load-displacement curves of the test specimens indicated that tensile membrane action was developed in the slab. Moreover, the second peak-carrying capacities of all specimens exceeded their first peak capacity; however, the punching failure will possibly prevent the development of the tensile membrane action.

6. The predicted dynamic effects for the test specimens ranged from 1.13 to 1.23, which were significantly less than those of 2 assumed in the design guidelines due to the test specimens being relatively ductile. However, correlated dynamic tests should be conducted in the future to more accurately evaluate their dynamic progressive collapse performance.

REFERENCES

1. ASCE/SEI 7, "Minimum Design Loads for Buildings and Other Structures," Structural Engineering Institute, American Society of Civil Engineers, Reston, VA, 2010, 424 pp.

2. UFC 4-023-03, "Design of Building to Resist Progressive Collapse," Unified Facility Criteria, U.S. Department of Defense, Washington, DC, 2009, 181 pp.

3. GSA, "Progressive Collapse Analysis and Design Guidelines for New Federal Office Buildings and Major Modernization Projects," U.S. General Service Administration, Washington, DC, 2003, 119 pp.

4. Marjanishvili, S., and Agnew, E., "Comparison of Various Procedures for Progressive Collapse Analysis," *Journal of Performance of Constructed Facilities*, V. 20, No. 4, Nov. 2006, pp. 365-374.

5. Gurley, C., "Plastic Disproportionate Collapse at Lost Corner," *Magazine of Concrete Research*, V. 61, No. 1, Feb. 2009, pp. 15-22.

6. Sasani, M., and Sagiroglu, S., "Progressive Collapse Resistance of Hotel San Diego," *Journal of Structural Engineering*, ASCE, V. 134, No. 3, Mar. 2008, pp. 478-488.

7. Yi, W.; He, Q.; Xiao, Y.; and Kunnath, S. K., "Experimental Study on Progressive Collapse-Resistant Behavior of Reinforced Concrete Frame Structures," *ACI Structural Journal*, V. 105, No. 4, July-Aug. 2008, pp. 433-439.

8. Orton, S.; Jirsa, J. O.; and Bayrak, O., "Carbon Fiber-Reinforced Polymer for Continuity in Existing Reinforced Concrete Buildings Vulnerable to Collapse," *ACI Structural Journal*, V. 106, No. 5, Sept.-Oct. 2009, pp. 608-616.

9. Su, Y. P.; Tian, Y.; and Song, X. S., "Progressive Collapse Resistance of Axially-Restrained Frame Beams," *ACI Structural Journal*, V. 106, No. 5, Sept.-Oct. 2009, pp. 600-607.

10. Yap, S. L., and Li, B., "Experimental Investigation of Reinforced Concrete Exterior Beam-Column Subassemblages for Progressive Collapse," *ACI Structural Journal*, V. 108, No. 5, Sept.-Oct. 2011, pp. 542-552.

11. Tian, Y., and Su, Y. P., "Dynamic Response of Reinforced Concrete Beams Following Instantaneous Removal of a Bearing Column," *International Journal of Concrete Structures and Materials*, V. 5, No. 1, June 2011, pp. 19-28.

12. Qian, K., and Li, B., "Slab Effects on Response of Reinforced Concrete Substructures After Loss of Corner Column," *ACI Structural Journal*, V. 109, No. 6, Nov.-Dec. 2012, pp. 845-856.

13. Qian, K., and Li, B., "Dynamic Performance of Reinforced Concrete Beam-Column Substructures under the Scenario of the Loss of a Corner Column—Experimental Results," *Engineering Structures*, V. 42, Sept. 2012, pp. 154-167.

14. Qian, K., and Li, B., "Experimental and Analytical Assessment on RC Interior Beam-Column Subassemblages for Progressive Collapse," *Journal of Performance and Constructed Facilities,* V. 26, No. 5, Oct. 2012, pp. 576-589.

15. Ellingwood, B. R.; Smilowitz, R.; Dusenberry, D. O.; Duthinh, D.; Lew, H. S.; and Carino, N. J., "Best Practices for Reducing the Potential for Progressive Collapse in Buildings," *NISTIR 7396*, National Institute of Standards and Technology, Department of Commerce, Washington, DC, 2007, 216 pp.

16. ABAQUS/CAE version 6.9, *Analysis User's Manual*, Dassault Systèmes, Springer, New York, 2009, 709 pp.

17. Sasani, M.; Bazan, M.; and Sagiroglu, S., "Experimental and Analytical Progressive Collapse Evaluation of Actual Reinforced Concrete Structure," *ACI Structural Journal*, V. 104, No. 6, Nov.-Dec. 2007, pp. 731-739.

18. Qian, K., "Experimental and Analytical Study of Reinforced Concrete Substructures Subjected to a Loss of Ground Corner Column Scenario," PhD dissertation, Nanyang Technological University, Singapore, Oct. 2012, 306 pp.

19. ACI Committee 318, "Building Code Requirements for Structural Concrete (ACI 318-08) and Commentary," American Concrete Institute, Farmington Hills, MI, 2008, 473 pp.

20. EN 1992-1-1, "Eurocode 2: Design of Concrete Structures—Part 1.1: General Rules and Rules for Buildings," Brussels, Belgium, 2004, 225 pp.

21. CEB-FIP MC90, "Design of Concrete Structures—CEB-FIP-Model Code 1990," Thomas Telford, London, UK, 1993, 437 pp.

22. DIN 1045-1, "Plain, Reinforced and Prestressed Concrete Structures—Part 1: Design and Construction," Normenausschuss Bauwesen (NABau) im DIN Deusches Institut fur Normung e.V. Beuth Verl. Berlin, Germany, 2001-07, 122 pp. (in German)

23. Gardner, N. J., "Verification of Punching Shear Provisions for Reinforced Concrete Flat Slabs," *ACI Structural Journal*, V. 108, No. 5, Sept.-Oct. 2011, pp. 572-580.

24. Guandalini, S.; Burdet, O. L.; and Muttoni, A., "Punching Tests of Slabs with Low Reinforcement Ratios," *ACI Structural Journal*, V. 106, No. 1, Jan.-Feb. 2009, pp. 87-95.

25. Abruzzo, J.; Matta, A.; and Panariello, G., "Study of Mitigation Strategies for Progressive Collapse of a Reinforced Concrete Commercial Building," *Journal of Performance of Constructed Facilities*, ASCE, V. 20, No. 4, Apr. 2006, pp. 384-390.